Non-steady experimental investigation on an integrated thermal management system for power battery with phase change materials

Authors: Shang Shi[a], Yongqi Xie[a,*], Ming Li[b], Yanping Yuan[c], Jianzu Yu[a], Hongwei Wu[d,], Bin Liu[b], Nan Liu[b]**

[a]School of Aeronautic Science and Engineering, Beihang University, Beijing, 100191, China
[b]Tangshan Railway Vehicle Co., Ltd., Tangshan, 063035, China
[c]School of Mechanical Engineering, Southwest Jiaotong University, 610031 Chengdu, China
[d]School of Engineering and Technology, University of Hertfordshire, Hatfield, AL10 9AB, United Kingdom

*Corresponding author. Email: xyq@buaa.edu.cn Tel. (86)10-82338081
**Corresponding author. Email: hongwei.wu@herts.ac.uk

Abstract: A large amount of heat inside the power battery must be dissipated to maintain the temperature in a safe range for the hybrid power train during high-current charging/discharging processes. In this article, a combined experimental and theoretical study has been conducted to investigate a newly designed thermal management system integrating phase change material with air cooling. An unsteady mathematical model was developed for the battery with the integrated thermal management system. Meanwhile, the heat generation power, thermal resistance, and time constant were calculated. The effect of several control parameters, such as thermal resistance, initial temperature, melting temperature and ambient temperature, on the performance of the integrated thermal management system were analyzed. The results indicated that: (1) the calculated temperature rise of the battery was in good agreement with the experimental data. The appropriate operation temperature of the battery was attained by the action of the phase change storage energy unit which is composed of copper foam and n-Eicosane, (2) the remarkable decrease of the battery temperature can be achieved by reducing the convection thermal resistance or increasing the conductivity of the phase change storage energy unit, where the latter could be the better option due to no additional energy

consumption. When convective resistance and thermal resistance between the battery surface and the phase change storage energy unit are less than 2.03 K/W and 1.85 K/W, respectively, the battery will not exceed the safety temperature under extreme condition, (3) the temperature rise declines with the decrease of the melting temperature or with the increase of the ambient temperature. It could be possible that the battery temperature exceeds the safety temperature for the high ambient temperature, (4) even if the phase change material is completely melted, the integrated thermal management system can still maintain the battery temperature within the safe range because of the air cooling.

Keywords: Integrated thermal management system; power battery; phase change material; air cooling; heat power.

Nomenclature

A	Heat exchange area (m^2)
B	Time constant (s)
Bi	Biot number
C	specific heat (J/(kg · °C))
E	Open-circuit (V)
h	Convective heat transfer coefficient (W/(m^2 · K))
I	Current (A)
L	Battery thickness (m)
q	Heat generation power of battery (W)
R	Thermal resistance (K/W)
T	Temperature (K)

T_D	Phase transition temperature (K)
T_∞	Ambient temperature (K)
t	Time (s)
U	Terminal voltage (V)
V	Volume (m^3)

Greek letters

ε	Emissivity
θ	Excess temperature (°C)
θ_0	Initial excess temperature (°C)
θ_D	Excess phase transition temperature (°C)
λ	Thermal conductivity (W/(m · K))
μ	Heat dissipation ratio of PCM and air cooling
ξ	The ratio of thermal resistance of air cooling and PCM
ρ	Density (kg/m^3)
σ	Stefan-Boltzmann constant
τ	Time step (s)
Φ	Heat transfer quantity (J)

Subscripts

h	Convection heat transfer
max	Maximum
p	Phase change
r	Radiation heat transfer

s The heat absorbed by the battery

Acronyms

DOD Depth of discharge

ITMS Integrated thermal management system

PCM Phase change material

PCSEU Phase change storage energy unit

SOC State of charge

TMS Thermal management system

1. Introduction

Compared to the traditional batteries such as lead-acid and nickel metal hydride, lithium-ion batteries has attracted much attention due to its characteristics of stable charge/discharge cycle, high power density [1], long lifespan, wide working temperature range, environment friendly and thus it has been widely used in hybrid electric vehicles and electric vehicles [2]. However, during the process of charge/discharge especially at large current, a large amount of heat will be generated due to various electrochemical and physical changes inside the battery. If the heat cannot be removed timely then it will accumulate inside the cells, which results in a sharp increase of the operating temperature inside the battery. This will further lead to an overheating, fire, or even explosion [3]. The previous research revealed that the performance and lifetime of the battery are strongly impacted by the operating temperature [4] and there should be an optimum operating temperature range and a maximum temperature difference in the battery pack [5]. In this case, an efficient thermal management system would be highly needed to dissipate the generated heat in order to obtain an ideal operating temperature and temperature uniformity.

A variety of thermal management system (TMS) have been reported in the open published literatures and many studies have been devoted to this area over the past decades. Zolot et al. [6] evaluated the thermal performance of the Prius NiMH battery pack which used the forced air cooling system. It was found that both the battery temperature and the temperature uniformity were maintained at an appropriate temperature range. Wu et al. [7] carried out a combined experimental and numerical study to investigate the temperature distribution in lithium-ion batteries. Their results showed that cooling by natural convection was not an effective means for removing heat from the battery system. It was also found that the forced convection cooling could mitigate temperature rise in the battery. Huo et al. [8] employed a mini-channel cold plate to cool the rectangular lithium-ion power batteries and the effects of the number of channels, flow direction, inlet mass flow rate and ambient temperature on the battery temperature rise were investigated. Zhao et al. [9] proposed a new kind of cooling method for cylindrical batteries based on mini-channel liquid cooled cylinder. It was found that the capacity of reducing the maximum temperature was limited through increasing the mass flow rate. The capacity of heat dissipation was enhanced first and then weakened along with the rising of entrance size. Khateeb et al. [10] designed a lithium-ion battery TMS with a novel phase change material (PCM). It was stated that the successful use of the PCM could be a potential candidate for the thermal management solution in electric scooter applications and for other electric vehicle applications. Rao et al. [11] experimentally and numerically discussed the thermal energy management performance of ageing commercial rectangular $LiFePO_4$ power batteries using PCM and thermal behavior related to the thermal conductivity between the

PCM and the cell. It was pointed out that it is necessary to improve the thermal conductivity and to reduce the melting point of the PCM for heat transfer enhancement.

In general, thermal management strategies of the battery can be divided into passive system and active system. The active TMS based on the forced air convection, liquid metal [12] or liquid cooling [13] with heat exchanger is always a routine solution. However, the drawback of the system is that it induces non-uniform temperature distribution in the battery pack with additional energy consumption. It has been reported that it consumed about 40% of the energy of the battery for the air TMS [14]. Whereas passive TMS using PCMs [15] or heat pipe [1] can decrease both the maximum temperature and the temperature difference within the battery pack. Meanwhile, there is no added energy consumption, which can significantly increase the available energy of vehicles. However, the traditional PCMs, such as paraffin, have low thermal conductivity which is in conflict with rapid heat storage. In order to overcome it, composite PCM is developed by adding high thermal conductivity materials, i.e. aluminum foam [16], copper foam [17], metal fins [10], or expanded graphite [18] into paraffin. Alipanah et al. [19] numerically investigated the TMS of the battery made from octadecane–Al foam composite materials. It was found that adding metal matrix of 0.88 porosity to the octadecane led to 7.3 times longer discharge time compared to the pure octadecane and increased the uniformity of the battery surface temperature. Wu et al. [20] developed a copper mesh composite as a composite PCM for battery thermal management. Copper mesh acted as a skeleton can further enhance both the thermal conductivity and strength of the whole module. Lin et al. [21] developed a passive TMS and applied the expanded graphite matrix and graphite sheets to compensate low thermal conductivity of PCM. Recently, with the increasing power of the battery module, single passive or active TMS is not competent to meet the requirements of battery temperature control. As a consequence, the combination of both active and passive systems has been developed as an effective measure. Zou et al. [22] presented an integrated thermal management system (ITMS) combining a heat pipe battery cooling/preheating system with a heat pump air conditioning system to fulfill the comprehensive energy utilization for electric vehicles. It was found that around 20% of the cooling capacity was supplied without increasing the input power. Tiari et al. [23] developed the discharging process of the thermal energy storage system which consisted of a square container, finned heat pipes, and potassium nitrate (KNO_3) as the phase change material. Charles-Victor et al. [24] developed a battery TMS coupling PCM (Rubitherm RT28 HC) with an active liquid cooling system in order to initialize the battery temperature at the melting of the PCMs during the charging process.

It is recognized that the heat generation power of the battery is a key parameter during the design of the TMS. There are two main experimental methods to study the mechanism of the battery heat generation, and they were isothermal microcalorimetry and accelerating rate calorimetry. Saito et al. [25] examined heat generation behaviors during the charge and discharge process for several commercial lithium-ion cells by using C-80 microcalorimeter and electrochemical device. Their results showed that the resistance of the battery increased after charging and discharging cycles, which led to the increase of the heat generation. In addition to the experiment, the establishment of the lithium-ion thermal model was another alternative to study the thermal behavior of the battery. The heat of the lithium-ion batteries mainly included the heat of reaction and the Joule heat [26]. Bernardi et al. [27] proposed a thermal model of heat generation rate based on the energy balance of the battery, and the developed model could be effectively applied to the analysis of the battery thermal characteristics. Sato [28] carried out a thermodynamics experiment for the lithium-ion batteries. A heat generation model of the battery, which was similar to that of Bernardi's thermal model, was also developed without considering the side reaction. And the contribution degree of the reaction heat value, polarization heat value, and Joule heat value was expressed quantitatively. The heat generation characteristic was dependent on the type of the battery. In most of the thermal management system, electric heater was normally used to simulate the battery heat generation for the purpose of the safety of the battery [29]. Due to different thermal conductivity and specific heat capacity between the electric heater and battery, the heater could not truly reflect the temperature characteristics of the battery prior to reaching the thermal balance.

It appears from the previous investigation that there were only limited reports on the theoretical research of the battery temperature rise, especially for the investigation on the TMS combining with more different cooling systems. In the present work, an ITMS with PCMs and air conditioning exhaust was designed for a lithium-ion power battery pack used in hybrid power train. The performances of the ITMS and pure air cooling system under different working conditions were investigated both experimentally and theoretically. The transient temperature rise model for the battery was derived and validated against experiment data. The heat generation power of the battery during the charge/discharge process was also calculated theoretically. In addition, the effects of several key parameters, such as thermal resistance, initial temperature, melting temperature and ambient temperature, on the performance of the ITMS were analyzed.

2. Non-steady model of temperature rise

It is recognized that the mechanism of the reaction and heat generation inside the battery are very complicated. As for the heat generation, it can be a function of the battery's properties, battery temperature, charge/discharge rate etc. Assuming that the internal enthalpy of the mixing and phase change can be neglected, the heat generation power of the battery is composed of reversible reaction heat and irreversible Joule heat, which can be expressed as follows[30]:

$$q = I\left[(E-U) - T\frac{\partial E}{\partial T}\right] \tag{1}$$

where $I(E-U)$ represents the irreversible Joule heat, $IT\frac{\partial E}{\partial T}$ is the reversible electrochemical reaction heat.

It should be noted that it is difficult to obtain accurate heat generation power by experiment in terms of Eq. (1). However, it could still be calculate based on the analysis of the heat transfer mode of the battery. For the case of air TMS, the internal heat (q) of the battery can be transmitted through three ways, namely, convective heat transfer (q_h), radiation heat transfer (q_r), and the battery storage heat (q_s). The Biot number (*Bi*) represents the ratio of the internal thermal resistance to the external thermal resistance. If there is no temperature difference within the battery during the whole process, it means that *Bi* is less than 0.1 and the battery heat transfer system is lumped-heat-capacity system [31]. When $Bi = hl/\lambda < 0.1$, the battery temperature will be only the function of time. Assuming that the specific heat of the battery (*c*) was constant during the charge and discharge [9], the governing equations of the heat dissipation of the battery can be described as:

$$q_h = \frac{(T-T_\infty)}{R_\mathrm{h}}, R_h = \frac{1}{hA_\mathrm{h}} \tag{2}$$

$$q_r = \varepsilon\sigma A(T^4 - T_\infty^4) \quad (3)$$

$$q_s = \rho c V \frac{dT}{dt} \quad (4)$$

$$q = q_\mathrm{h} + q_\mathrm{r} + q_\mathrm{s} \quad (5)$$

where T (K) is the temperature of the battery, T_∞ (K) is the ambient temperature, A (m^2) is the heat exchange area, ρ (kg/m^3) is the density of the battery, V (m^3) is the volume of the battery.

The period of the charge/discharge can be divided into several discrete time steps (τ). If τ was small enough, q can be assumed to be constant in the current time step. In the current experiment, τ is equal to the interval time of the data acquisition. Therefore, by ignoring the radiation heat transfer [8], the energy balance of the battery with its analytic solution can be obtained:

$$\rho c V \frac{dT}{dt} = q - \frac{(T - T_\infty)}{R_\mathrm{h}} \quad (6)$$

$$\frac{qR_\mathrm{h} - \theta}{qR_\mathrm{h} - \theta_0} = \exp\left(-\frac{1}{\rho c V R_\mathrm{h}} t\right) = \exp\left(-\frac{t}{B}\right), \quad 0 \leq t \leq \tau \quad (7)$$

where qR_h is equal to the maximum temperature or stable temperature of the battery (θ_max), θ_0 and θ are the excess temperatures of batteries at $t = 0$ and $t = t$, respectively, R_h is the convective thermal resistance, $B = \rho c V R_\mathrm{h}$ is the time constant that denotes the response speed of the battery temperature change.

When $q = 0$, the equation of the battery temperature rise is written as:

$$\frac{\theta}{\theta_0} = \exp(-\frac{t}{B}) \quad (8)$$

The variation of the battery temperature with time can be experimentally obtained during the air cooling process without charge/discharge, and then the time constant (B) can thus be calculated according to Eq. (8). Combined with experimental data of temperature distribution with charge/discharge, q and its total heat transfer quantity (Φ) can be calculated as follows:

$$q = \frac{1}{R_\mathrm{h}}\left(\frac{\theta-\theta_0}{1-\exp(-\frac{t}{B})} + \theta_0\right) \tag{9}$$

$$\Phi = \int_0^t q\, dt \tag{10}$$

Compared with air TMS and ITMS, PCM provides additional cooling load. Assuming that the PCM gained the heat in the form of the latent heat, when the thermal resistance (R_p) between the battery and the PCM is constant, the heat absorbed by the PCM (q_p) is given by the form

$$q_\mathrm{p} = \frac{T-T_\mathrm{D}}{R_\mathrm{p}} \tag{11}$$

Similar to Eqs. (6) and (7), the thermal balance with its analytical solution in the ITMS can be expressed as follows:

$$\rho c V\frac{dT}{dt} = q - \frac{(T-T_\infty)}{R_\mathrm{h}} - \frac{T-T_\mathrm{D}}{R_\mathrm{p}} \tag{12}$$

$$\frac{(\frac{1}{R_\mathrm{h}}+\frac{1}{R_\mathrm{p}})(\theta-\theta_0)}{q-\frac{1}{R_\mathrm{h}}\theta_D-(\frac{1}{R_\mathrm{h}}+\frac{1}{R_\mathrm{p}})(\theta_0-\theta_\mathrm{D})} = 1-\exp\left(-\frac{\frac{1}{R_\mathrm{h}}+\frac{1}{R_\mathrm{p}}}{\rho c V}t\right) \tag{13}$$

where $\theta_D = T_D - T_\infty$ is the excess phase change temperature. Let $\xi = \frac{R_\mathrm{h}}{R_\mathrm{p}}$, Eq. (13) can be further reduced to

$$\frac{(1+\xi)(\theta-\theta_0)}{qR_\mathrm{h}+\xi\theta_\mathrm{D}-(1+\xi)\theta_0} = 1-\exp\left(-\frac{1+\xi}{B}t\right) \tag{14}$$

According to Eq. (13), the key parameters of the ITMS include the ambient temperature, the phase change temperature, the heat generation of the battery, the convective thermal resistance, the conduction resistance and the initial temperature of the battery.

For the ITMS, it can be divided into two independent cooling modes, they are air-cooling mode and phase-change cooling mode. In order to explore which mode is dominant, the ratio (μ) is defined as the following:

$$\mu = \xi(1 - \frac{\theta_D}{\theta}) \tag{15}$$

If $\mu > 1$, it means that the PCM will absorb most of the heat load. Whereas if $\mu < 1$, it implies that the air will remove the major heat load. When $\mu = 1$, the effect of both cooling modes is equal. When q, R_h and R_p are known, the battery temperature characteristics of the ITMS can be predicted by Eq. (14).

3. System description and experimental setup

A new experimental test rig was constructed at Reliability and Environmental Engineering Laboratory at Beihang University, China to investigate the thermal management performance of the power battery with ITMS.

3.1. System description

Fig. 1 shows a schematic diagram of the ITMS with PCM. The ITMS mainly consists of four phase change storage energy units (PCSEU) which were arranged on one side of the battery pack. The PCSEUs were assembled in connection with the thick copper sheets with dimension of 2 mm×15 mm×80 mm. The battery pack was formed by using thirteen porous structures (engineering plastic-ABS) and twelve lithium-ion cells covered with a 0.37 mm aluminum sheet, which was 1/48 of the real battery pack in hybrid power train. The battery will be cooled by air through the porous structure and it was not affected by the PCSEU. The PCSEU absorbed the heat by heat conductivity. In order to enhance the thermal conductivity of the PCM, the PCSEU was made up of 95% foam copper and paraffin. The n-Eicosane with purity of 99% was employed as the organic PCM and its fusion point is from 36 ºC to 38 ºC. To make sure that the battery was the main heat source, the thermal insulation material (Rubber Foam Thermal Insulation Sheet, 0.034 W/m·K) was covered on the surface of the PCSEU to reduce the influence of the external air convection. Additionally, in order to quantitatively describe the performance of the ITMS, the TMS with pure air cooling was also assembled as a reference. Fig. 2 illustrates the test section of the experimental study. The details of the battery properties provided by the battery manufacturer are listed in Table 1. To determine the convective heat transfer coefficient and the heat transfer resistance of the battery and the PCM, the batteries in the battery pack can be replaced by the electric heaters directly due to the same size.

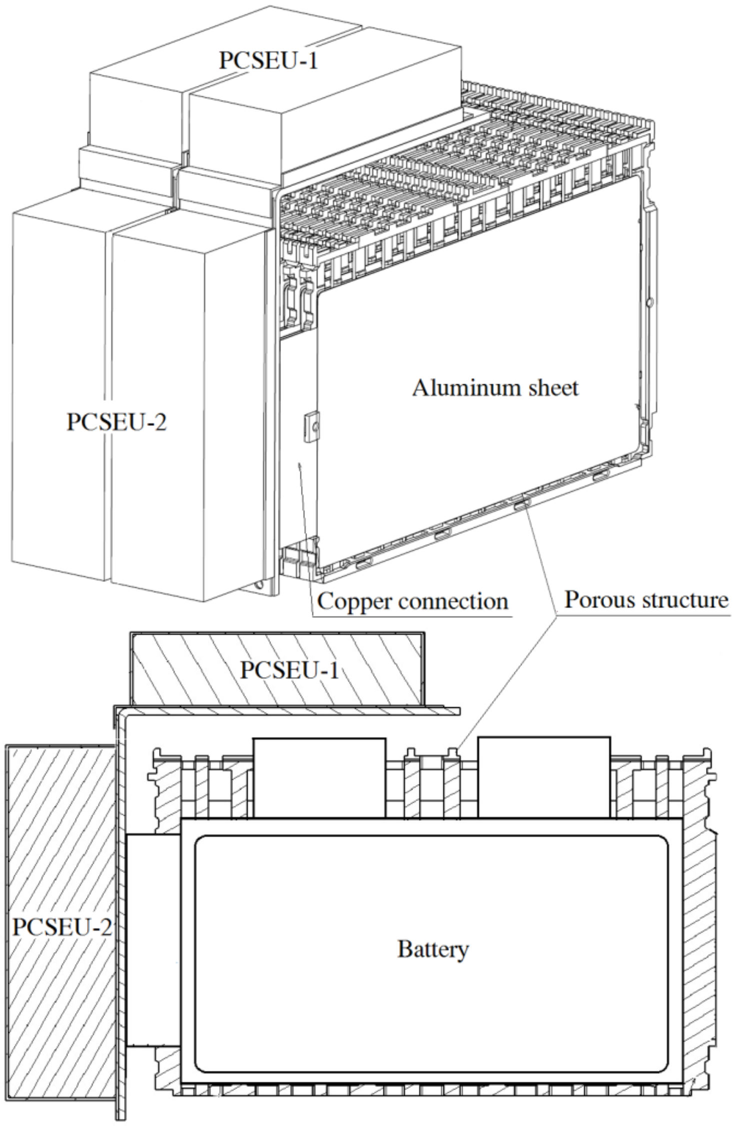

Fig. 1. The schematic diagram of the ITMS with PCM.

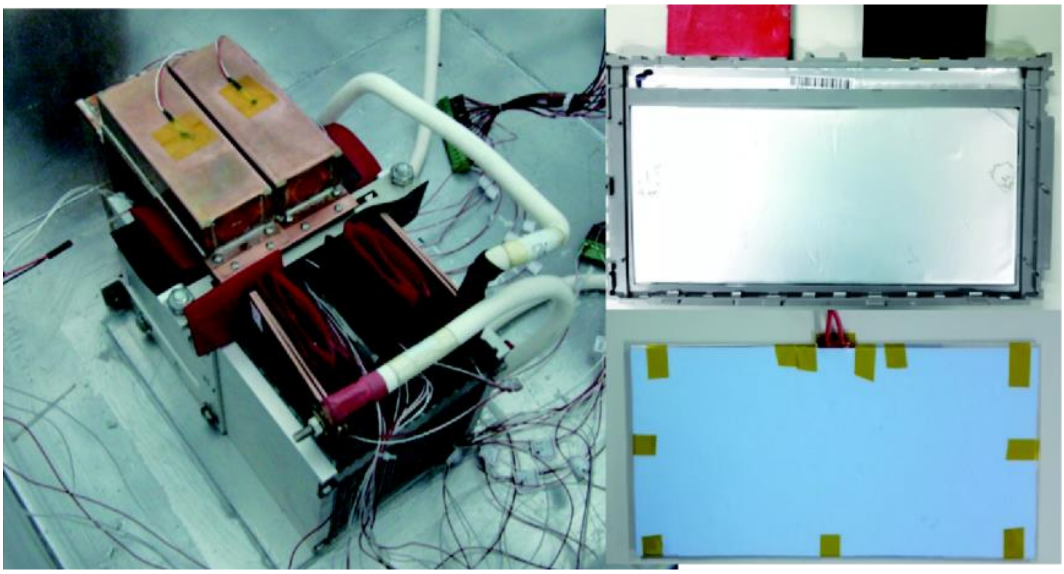

Fig. 2. Test section.

Table 1 Information of the cell.

Item	Value (unit)
Type	Lithium titanate battery
Size	6.1×203×127 (mm×mm×mm)
Nominal voltage	2.3 V
Capacity	10 Ah
Recommended temperature	-10 ~ +45 ºC(charge) -25 ~ +55 ºC(discharge)
Thermal conductivity of battery	5.22 W/(m·K)

3.2. Experimental setup

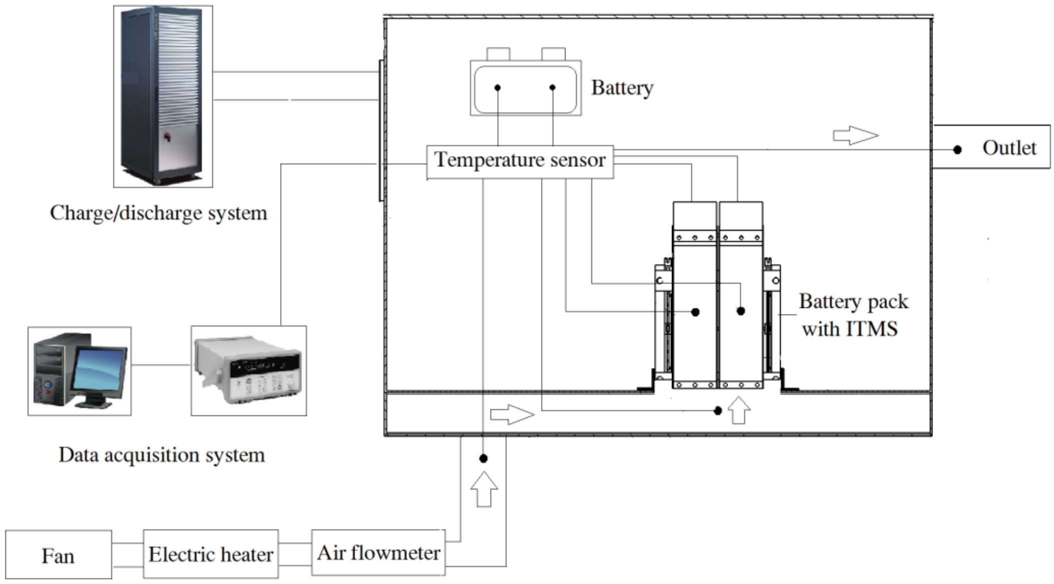

Fig. 3. Schematic diagram of the experimental apparatus.

The schematic diagram of the experimental apparatus is illustrated in Fig. 3. The main components of the system consist of thermal performance test system, the charge/discharge system and the data acquisition system. During the discharge process, the battery pack was discharged to the 18 V with constant current (2C/20 A, 3C/30 A and 4C/40 A). While during the charge period, the battery pack was charged to the termination voltage (33.6 V) under three separate rates (2C, 3C and 4C), and then charged at 33.6 V until the termination current (0.5 A). For the thermal performance test system, a frequency conversion fan and electric heater were used to regulate the air flow and temperature, respectively. An air flowmeter measures the flow rate from 0.5 N m^3/h to 50 N m^3/h (50±0.25 N m^3/h). The pipe system ensured that the air flowed through the stack with minimum pressure loss. In order to prevent the internal air from being heated by the external environment, the thermal insulation materials (Rubber Foam Thermal Insulation Sheet, 0.034 W/m·K) were covered on the surface of the pipe. In the current work, three different inlet air temperatures of 28 ^{o}C, 35 ^{o}C and 42 ^{o}C were selected to simulate the exhaust air of air condition, the mixed air and the natural air in summer. Platinum temperature sensors were used (±0.06 °C at 0 °C). The temperatures at different locations were recorded every second by using the Agilent 34970A, as shown in Fig. 3.

4. Results and discussion

In the current study, the temperature rise characteristics of the battery with air cooling system were discussed in under the air flow rate of 18 m^3/h and the natural convection. The performance of the ITMS was described in comparison with the air cooling system. Comparsion between the experimental data and the calculated results is achieved, and the parameters that affecting the performance of the ITMS and the approach for battery temperature reduction were investigated in detail.

4.1. Test with air cooling system

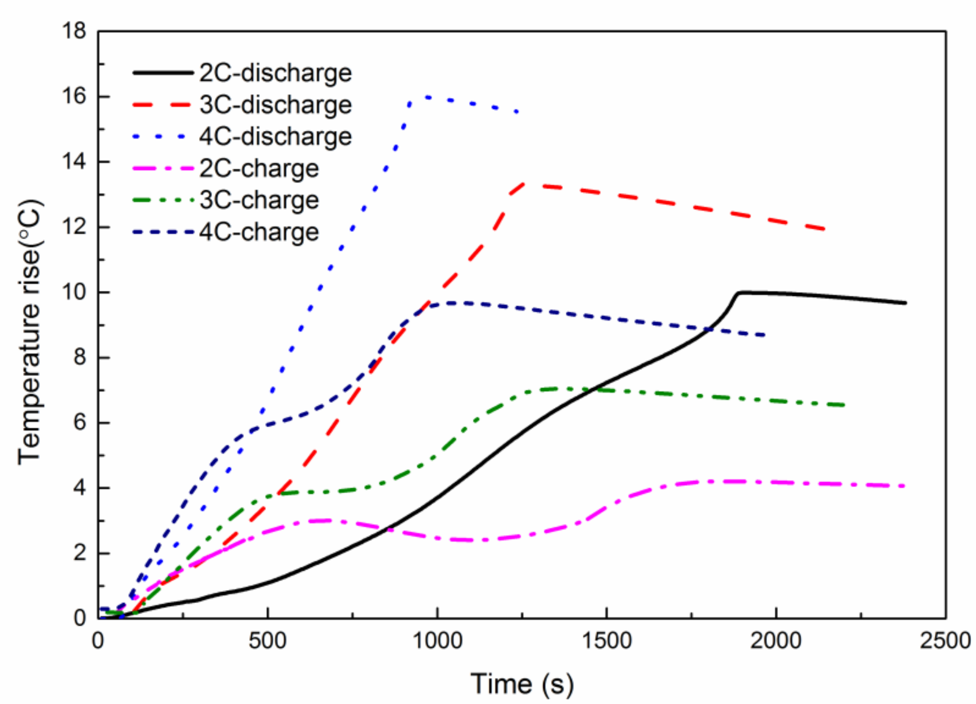

Fig. 4. Temperature rise of the battery pack without PCM under natural convection at ambient temperature of 28 °C.

Fig. 4 shows the temperature rise of the battery pack with air cooling system only for 2C, 3C and 4C charge/discharge rates. In the current study, the temperature rise means that the temperature of the battery exceeds the ambient temperature. It could be found that the temperature of the cell did not reach a steady state until the end of the charge/discharge. It can be seen clearly from Fig. 4 that, when the initial temperature rise of the battery was 0 $^{\circ}$C, the maximum temperature rise of 4C discharge was 16.2 $^{\circ}$C, which was larger than that of the other cases. This demonstrates that the charge/discharge current can significantly impact on the temperature rise of the battery. It was noted that the battery temperature did not exceed the safety temperature of 55 $^{\circ}$C in this case. For the case of the charge process, the decrease of the temperature rise rate appeared in the charge intermediate stage due to the interaction between the reaction and Joule heating inside the battery. It caused that the highest temperature at the end of charge was less than that of the discharge process.

Table 2 The comparison of the maximum temperature rise at natural convection and air flow rate of 18 m^3/h.

Case	18 m^3/h		Natural convection		Percentages of decline
	Initial temperature	Initial temperature	Initial temperature	Maximum temperature	
2C-charge	3	3.9	0	4.1	7.1%
3C-charge	4	6.8	0	7.0	2.9%
4C-charge	6	8.9	0	9.2	3.3%
2C-discharge	0	7.1	0	9.9	28.3%
3C-discharge	0	10.5	0	13.2	20.5%
4C-discharge	0	12.5	0	16.2	22.8%

When the air flow rate was 18 m^3/h and the ambient temperature was 28 $^{\circ}$C, as shown in Table 2, it could be found that the temperature rise of the battery pack decreased owing to the large convective heat transfer coefficient. Due to the battery was not cooled to the ambient temperature, different initial temperatures appeared during the charging process. Compared with the natural convection, for the case of the charge process at 18 m^3/h, the percentages of decline of the maximum temperature rise were 7.1%, 2.9% and 3.3% with the initial temperature rises of 3 ^{o}C, 4 ^{o}C and 6 ^{o}C, respectively. In comparison, for the discharge process, it had more than 20% decline which was much higher than that of the charge process. It was indicated that the high initial temperature wourld result in the high final temperature of the battery.

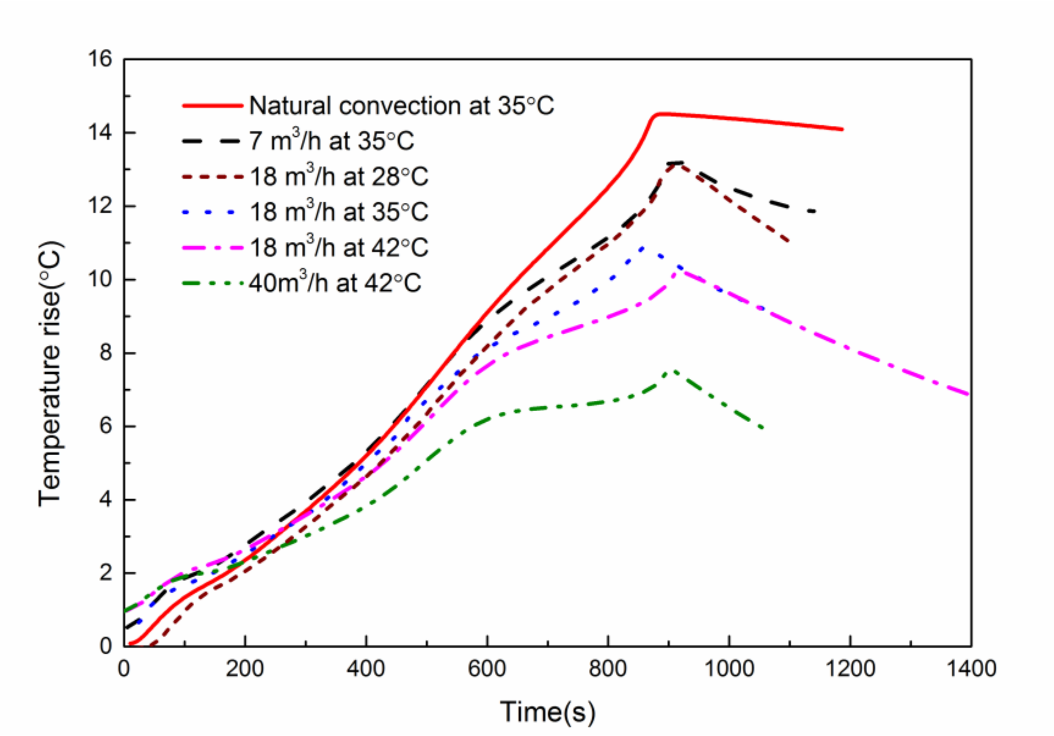

Fig. 5. Temperature rise of the battery pack for 4C discharge rate at different air flow rates and ambient temperatures.

Fig. 5 shows the variation of the temperature rise for 4C discharge rate at different air flow rates and ambient temperatures. It was noted that the maximum temperature rise was 14.5 ^{o}C under natural convection at the ambient temperature of 35 ^{o}C, which was 1.7 ^{o}C less than that of 28 ^{o}C. But considering the influence of the ambient temperature, the highest temperature of the battery reached 49.5 ^{o}C which was higher than that of 28 ^{o}C. Under the flow rate of 18 m^3/h, the maximum temperature rises at 28 ^{o}C, 35 ^{o}C and 42 ^{o}C were 12.5 ^{o}C, 11 ^{o}C and 10.2 ^{o}C, respectively. It implied that there was little difference of heat generation between 35 ^{o}C and 42 ^{o}C. Despite this, the highest temperature of the battery at 42 ^{o}C was about 52.2 ^{o}C, which is very close to the safety temperature. As a result, a high ambient temperature can restrain the maximum temperature rise of the battery, but could easily induce the battery temperature approaching the safety temperature. Therefore, batteries at high ambient temperature are not desirable.

It is always the case that a non-uniform flow field can potentially result in a non-uniform temperature distribution inside the battery pack for the case of air cooling. During the experiment, when the air flow rate was 40 m^3/h and the ambient temperature was 42 ^{o}C, the maximum temperature rise was 7.6 ^{o}C at the end of discharge. Considering the safety issue of the battery, the test was not carried out for the case of the air flow rate of 7 m^3/h and the ambient temperature of 42 ^{o}C. However, it could be evaluated that the maximum temperature rise in this case was close to or even exceeded 13.2 ^{o}C based on the experimental data. This means that the temperature difference could be larger than 5 ^{o}C inside the battery pack. Consequently, the non-uniform temperature distribution increased the chance of capacity fade of battery system and further affected the overall lifespan of the battery. In addition, it would be recommended that the ambient temperature should not exceed 35 ^{o}C when taking the energy saving and the safety of the battery into account.

4.2. Performance analysis of ITMS with PCM

According to the results for the air cooling system discussed in Section 4.1, the temperature performances of the ITMS with PCM were discussed only for the cases of 3C and 4C.

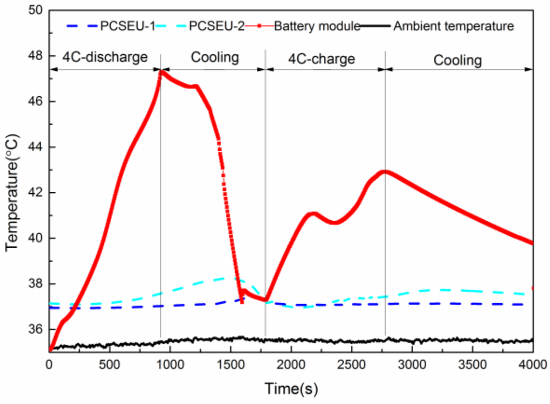

(a) 35 °C /natural convection

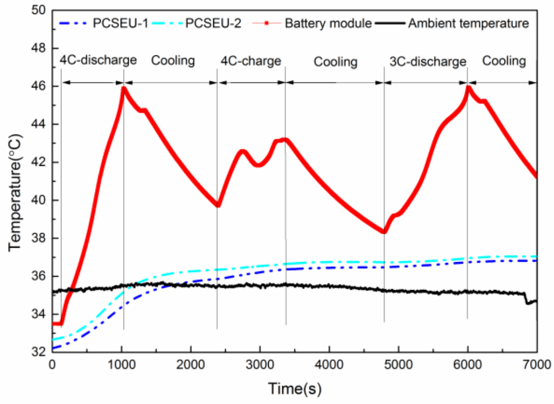

(b) 35 °C /7 m^3/h

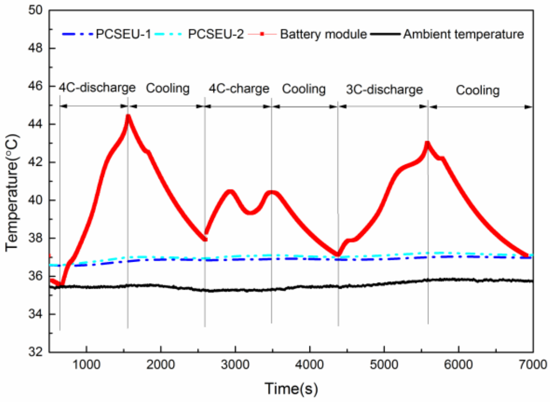

(c) 35 °C /18 m^3/h

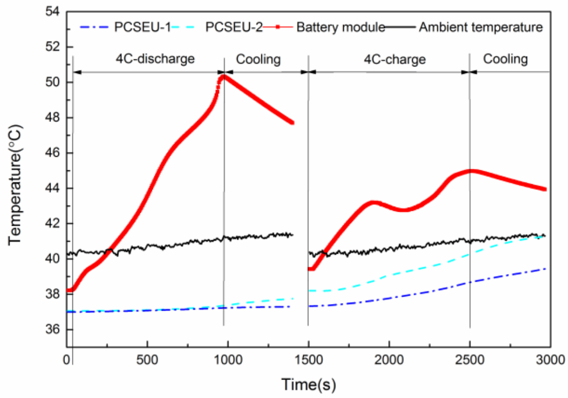

(d) 42 °C /7 m^3/h

Fig. 6. Temperature variation of ITMS at 4C and 3C discharging and charging process under different conditions: (a) 35 °C /natural convection; (b) 35 °C/7 m^3/h; (c) 35 °C/18 m^3/h; (d) 42 °C/7 m^3/h.

Fig. 6 presents the surface temperature of the battery pack with the ITMS under natural convection and forced convection conditions. During the tests, the air flow rates of both 7 m^3/h and 18 m^3/h were set and the ambient temperature were 35 °C and 42 °C, respectively. As illustrated in Fig. 6(a), the highest temperatures for the case of natural convection at the end of 4C discharge and charge process reached 47.4 °C and 43 °C with the temperature rise of 12.4 °C and 8 °C. Compared with the case without PCM, as shown in Fig. 5, there was more than 2.6 °C of temperature drop at 4C discharge rate for the ITMS. This indicates that the PCMs provide additional heat dissipation due to the solid paraffin melts to store heat for the latent heat.

During the cooling process after the discharge/charge, the residual heat induced that the PCMs were still heating up slowly till the temperature of the battery was lower than that of the PCMs. The difference of the curves for the cooling process was due to the utilization of the air forced convection cooling only after 4C discharge. Overall, the battery temperature did not exceed the safe temperature (55 ^{o}C /discharge and 45 ^{o}C /charge). It could be attributed to the ITMS.

For the case of 4C discharge rate, as demonstrated in Fig. 6(b), the highest temperature of the battery was 46 ^{o}C with the maximum temperature rise of 11 ^{o}C as the air flow rate was 7 m^3/h. This value was nearly the same as the highest temperature for the case of 7 m^3/h presented in Fig. 5. In addition, it should be noted that the temperature of the PCMs did not reach the melting point (36 ^{o}C). This implied that the heat was stored as the form of the sensible heat. During the cooling period after 4C discharge, the surface temperature of the battery underwent a sharp temperature drop. At the same time, the temperature of PCM was slowly heated to the melting point. For the case of 4C charge process, the highest temperature of the battery was 43.2 ^{o}C with the coupled action of the cooling air and the PCMs. But there was only 0.3 ^{o}C lower than that for the case of natural convection and 35 ^{o}C due to the higher initial temperature. As a result, the initial temperature has a significant influence on the battery under the unsteady state heat transfer process. Similarly, because the initial temperature of 3C charge was much higher than that of 4C discharge, their highest temperatures were all about 46 ^{o}C. Therefore, the higher initial temperature of the battery plays a negative role in the battery temperature rise.

For the case of 18 m^3/h and 35 ^{o}C as shown in Fig. 6(c), the surface temperature of the battery reached 44 ^{o}C with the maximum temperature rise of 9.5 ^{o}C at the end of the 4C discharge process. Based on the above analysis, the highest temperature of the battery decreased with the increase of the air flow rate. Under the large flow rate for the ITMS, air forced convection cooling dominated the heat dissipation and the function of the PCSEU was degraded. For the case of 4C charge process, it could be found that there were two temperature peaks with almost the same value. The temperature drop in the intermediate stage was the result of the domination of the heat dissipation relative to the heat generation of the battery.

In Fig. 6(d), since the 4C charge and discharge cycles were not carried out continuously, the temperature curve during the air cooling period was interrupted. For the 4C discharge process, the highest temperature of the battery was 50.3 ^{o}C. The temperature of the PCSEU was more than 36 ^{o}C, which means that the PCMs absorbed the heat in the form of latent heat effectively. By contrast with the case of pure air cooling, the ITMS expands the safety of the battery for smaller flow rate. During the 4C charge period, the highest surface temperature was 44.8 ^{o}C after the PCM was completely melted. This was due to the PCSEU did not have a negative impact on the air cooling and the air cooling still can remove the majority of the heat. Meanwhile, the battery has a risk of exceeding 45 ^{o}C. Consequently, measurement need to be taken to improve the reliability of the ITMS, such as reducing the battery initial temperature and the ambient temperature, increasing the air flow rate during the charge process.

4.3. Analysis of influencing factors

As described previously, the temperature characteristics of the battery are affected by several control factors, such as heat generation power, battery properties, ambient temperature and initial temperature. In this section, the convection resistance and time constant were calculated firstly. Then the heat generation power was evaluated. Combined with the thermal resistance of the heat absorption of PCM, the veracity of the mathematic model is verified against experimental data. Furthermore, the influence of these parameters on the characteristics of the ITMS was analyzed in a systematic manner.

4.3.1. Parameters calculation

Table 3 shows the stable temperature of the electric heater at different power under the natural convection and forced convection conditions with air flow rate of 18 m^3/h. In the current study, it was assumed that the physical parameters of the cooling air were constant during the temperature range from 28 °C to 42 °C, the average convective resistances (R_h) can be obtained according to Eq. (2), which were 13.87 K/W and 2.12 K/W at natural convection and forced convection (18 m^3/h), respectively.

Table 3 Average convective resistances for the natural convection and forced convection.

Case	Input power/W	Stable temperature/ °C	Ambient temperature/ °C	Average convective resistance/ K/W
Natural convection	2	48.4	20.0	13.87
	3	60.8	19.9	
	4	75.4	19.8	
	5	88.1	19.6	
Forced convection /18 m^3/h	2	24.1	19.9	2.03
	3	25.8	19.8	
	4	27.9	19.8	
	5	30.2	20.1	

Furthermore, *Bi* could be calculated based on the average convection resistances. For the case of the natural convection, *Bi* was equal to 0.004, while for the forced convection, *Bi* was equal to 0.027. It inferred that the internal thermal resistance of the battery could be ignored. Consequently, according to Eq. (8) and the battery temperature drop as shown in Fig. 7, the reciprocal of the time constant (1/*B*) under different operating conditions can be calculated, as listed in Table 4.

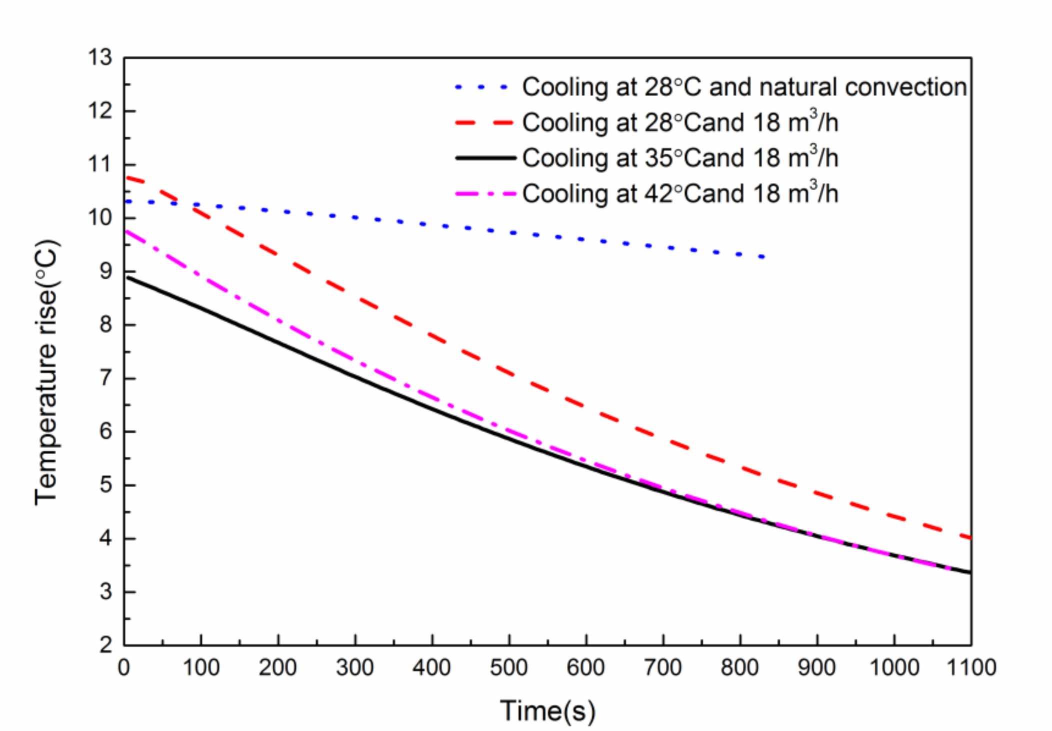

Fig. 7. The battery temperature drop under different operating conditions.

Table 4 The value of 1/*B*

Case	1/*B* (s^{-1})
T28-F0	1.4×10^{-4}
T28-F18	9.5×10^{-4}
T35-F18	9.3×10^{-4}
T42-F18	9.7×10^{-4}

✶T28-F18 means that the ambient temperature is 28 °C and the air flow rate is 18 m^3/h.

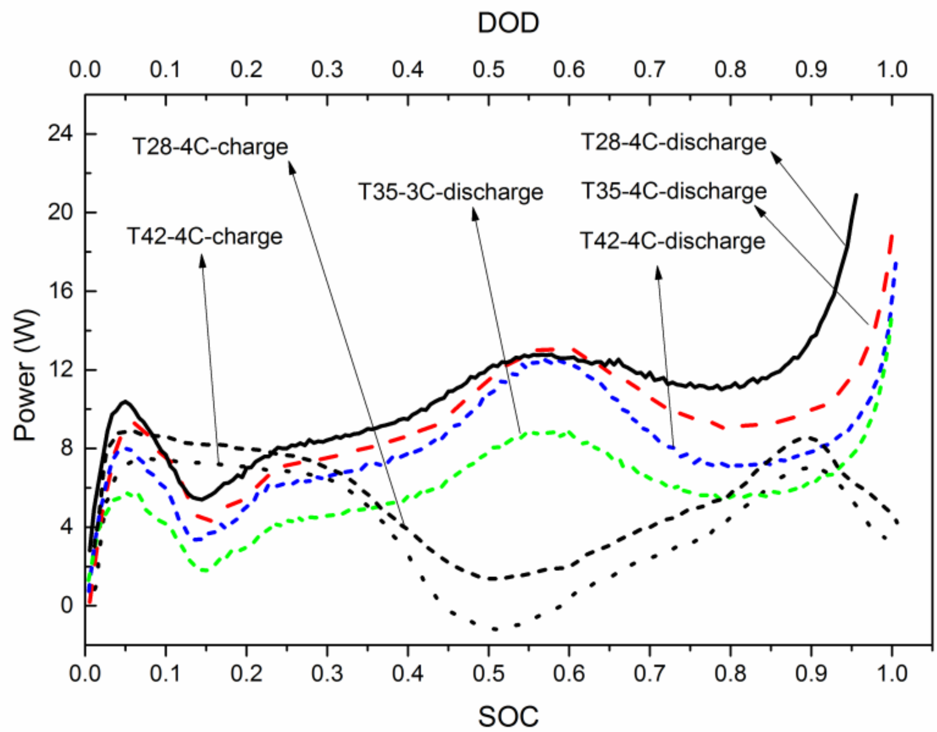

Fig. 8. Variation of power of the battery heat generation with state of charge and depth of discharge.

Fig. 8 shows the power of the battery heat generation with state of charge (SOC) and depth of discharge (DOD) at ambient temperatures of 28 °C, 35 °C, and 42 °C, which is calculated in terms of Eq. (9). During the discharge process, there were three power peaks at DOD=0.05, 0.56 and 1.0, respectively. The small heat power appeared at DOD=0.14 after the steep decline. For the case of 4C discharge at different ambient temperatures, the battery had nearly the same heat power at the initial stage (DOD<0.05). When DOD> 0.05, the heat powers at 28 °C was higher than that of 35 °C and 42 °C. It could be used to explain why the battery at 28 °C has a highest temperature rise. When DOD>0.9, the heat power increased rapidly. On the other hand, it was obvious that the decrease of the current reduction can significantly reduce the battery heat power in comparison with 4C and 3C discharge at 35 °C. For the case of the charge process, there were two heat power peaks at SOC=0.05 and 0.9. The heat power curve has a great depression at intermediate states of the discharge and the minimum value appeared at

SOC=0.5. The negative heat power indicated that the heat absorption of the electrochemical reaction was more than that of the Joule heat, which caused the temperature drop. Similar to the discharge process, the heat power at 42 ^{o}C was lower than that of 28 ^{o}C. Due to the charging current gradually decreased during the constant voltage charging process at the end of charge, the heat power rapidly declined.

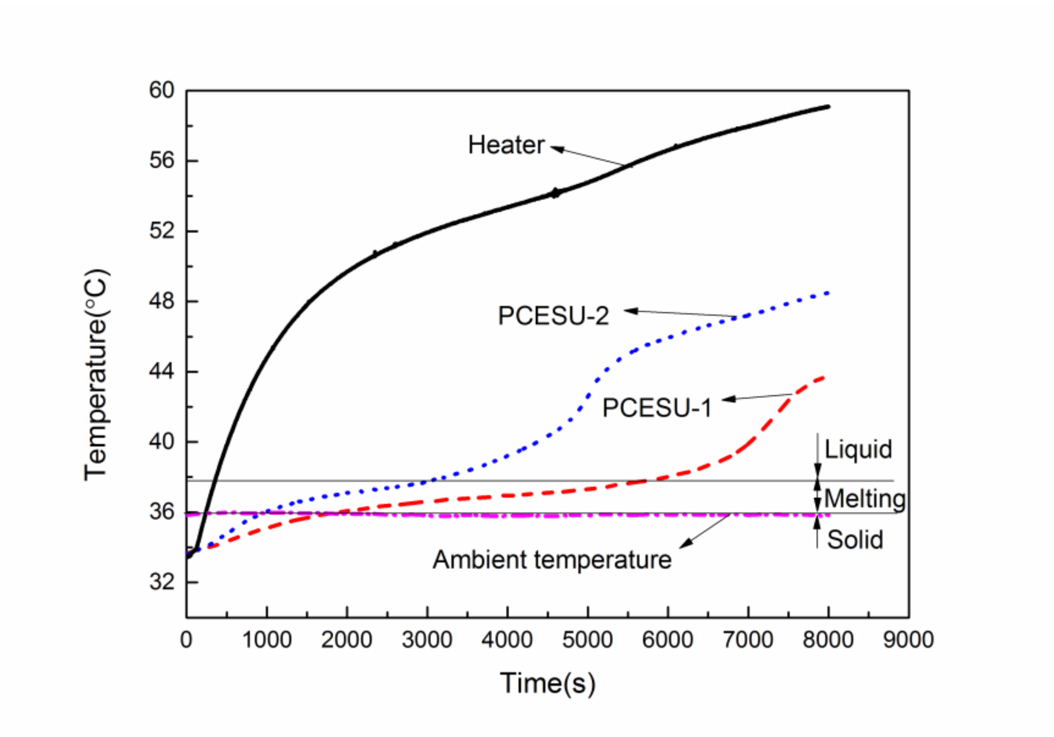

Fig. 9. Temperature variation of electric heater with time at 5 W.

Fig. 9 shows the temperature variations of the electric heater under natural convection at the heat load of 5 W. The melting temperature (T_D) range is from 36 ^{o}C to 37.8 ^{o}C. As the PCESU-2 was close to the heat source, it melted completely with less time. The increase of the surface temperature of the PCESU was attributed to the increase of the thermal resistance (R_p) between the cell and solid-liquid interface inside the PCESU with the melting of the PCMs. It was different from the assumption in Eq. (13) that the thermal resistance was constant. In order to simplify the calculation and modify the thermal resistance, the melting temperature was fixed to 36.9 ^{o}C in the current study, thus the thermal resistance could be calculated as 3.90

K/W by Eq. (13). Obviously, increasing the thermal conductivity of the PCM can reduce the internal thermal resistance of the PCSEU and effectively improve the accuracy of the thermal resistance.

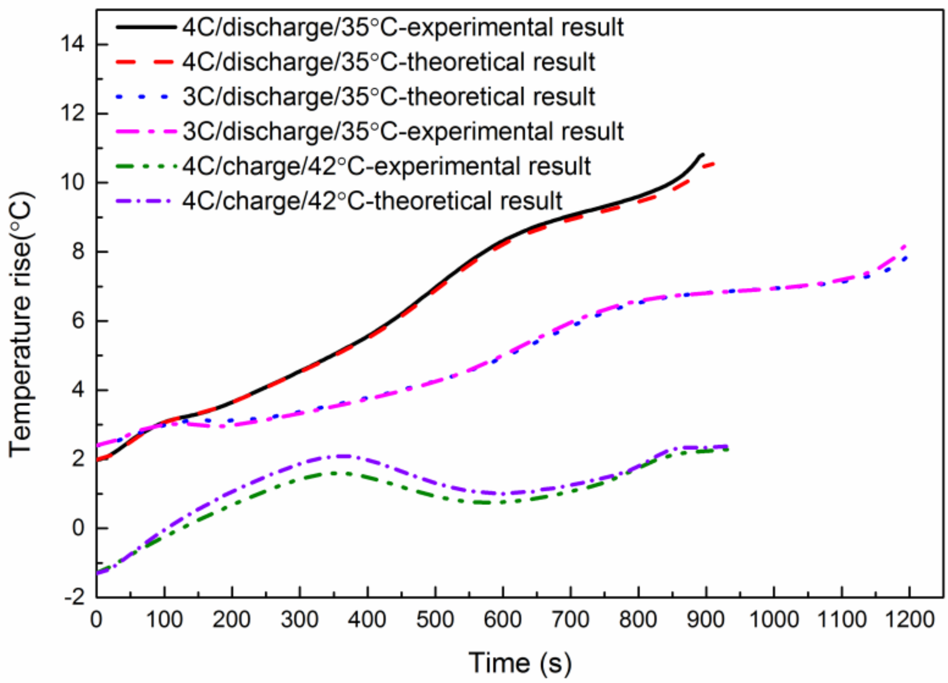

Fig. 10. Comparison between theoretical results and experimental data of the ITMS.

Fig. 10 shows the comparison of temperature rise between experimental data and theoretical results calculated by Eq. (14) at ambient temperatures of 35 °C and 42 °C under the flow rate of 18 m^3/h. For the 4C and 3C discharge process, the parameters used in Eq. (14) were ξ=0.52 and B^{-1}=0.00093. For the case of the 4C charge process, ξ=0.52 and B^{-1}=0.00097 were selected. It was found that good agreement between the experimental data and the theoretical results was achieved. The maximum error was around 3.33%, which was mainly due to the fixed thermal resistance.

4.3.2. Effect of initial temperature

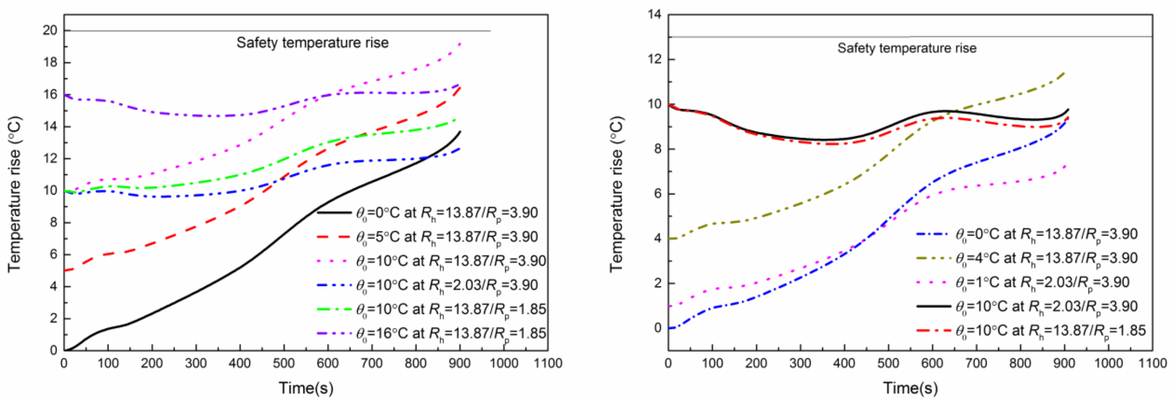

(a) 35 °C (b) 42 °C

Fig. 11. The effect of initial temperature at different ambient temperatures: (a) 35 °C; (b) 42 °C.

The influence of the initial temperature at two different ambient temperature of 35 °C and 42 °C are shown in Fig. 11. The air natural convection and forced convection with flow rate of 18 m^3/h were compared. θ_0 expresses the temperature that the initial temperature of the battery exceeds the ambient temperature while 0 m^3/h expresses natural convection. When the ambient temperature was 35 °C, as shown in Fig. 11(a), it could be found that a higher initial temperature resulted in a larger final temperature of the battery. Especially when θ_0 was higher than 10 °C, the temperature rise was close to the safety value under natural convection condition and R_p=3.9 K/W. For the case of natural convection, decreasing the R_p from 3.9 K/W to 1.85 K/W, the PCMs exerted their roles to maintain the battery temperature within safe range even at θ_0=16 °C. For the air forced convection case (R_h=2.03 K/W), the maximum temperature rise did not exceed 12 °C and the battery temperature located in the safety temperature range.

During the discharge process under natural convection condition at 42 °C, as shown in Fig. 11(b), the temperature rise approached 55 °C when θ_0 was equal to 4 °C. For the case of 18 m^3/h, the temperature rise tended to keep in a horizontal level under the safe range when θ_0=10

^{o}C. The same effect can be achieved by reducing the thermal resistance from the 3.9 K/W to 1.85 K/W under natural convection. Consequently, it was at R_h=2.03 K/W or R_p=1.85 K/W that the maximum temperature of the battery could maintain within 55 ^{o}C under higher initial temperature. Despite this, lower initial temperature is always beneficial to reduce the maximum temperature under the unsteady heat transfer process, whereas higher initial temperature is not desirable.

4.3.3. Effect of thermal resistance

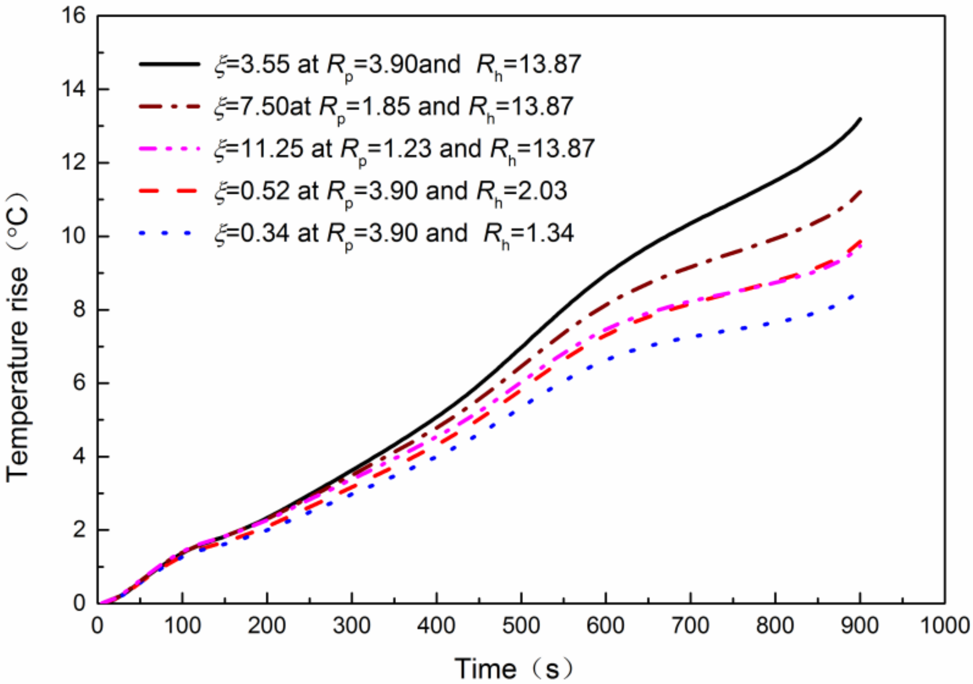

Fig. 12. Temperature rise at different R_h and R_p.

Fig. 12 shows the temperature rise at different thermal resistances of both R_h and R_p at ambient temperature of 35 ^{o}C. When R_h was 13.87 K/W, the maximum temperature rise reduced from 13.7 ^{o}C to 10.0 ^{o}C due to the decrease of R_p from 3.90 K/W to 1.23 K/W. Lower R_p resulted in extra heat absorption of PCM. The convective thermal resistance is directly related to the wind speed and the heat transfer area. For a fixed thermal resistance (R_p=3.90 K/W), when the convective thermal resistance decreases from 2.03 K/W to 1.34 K/W, the highest temperatures rise were 9.9 $^{\circ}$C and 8.2 $^{\circ}$C, respectively. Similarly, the temperature drop was caused when the R_p decreases from 1.85 K/W to 1.23 K/W. Therefore, either to reduce the PCM thermal resistance or reduce convective thermal resistance can play a positive role in reducing the surface temperature of the battery.

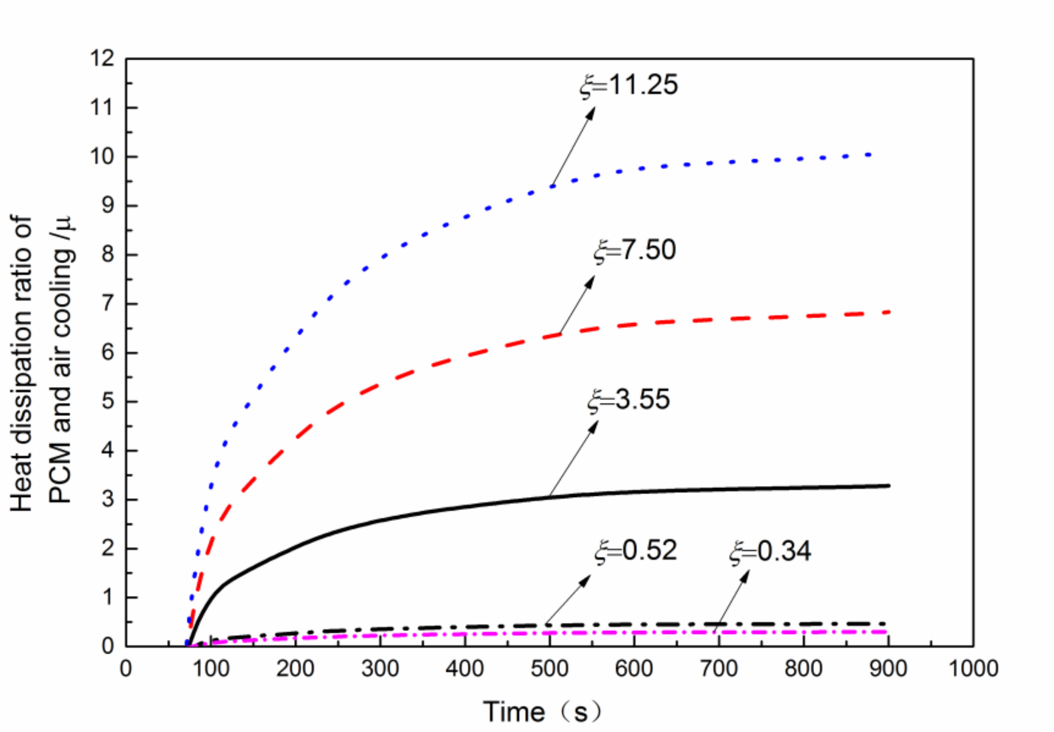

Fig. 13. Heat dissipation Ratio of the PCM and air cooling at different ξ.

It appears from the previous experimental investigations that the battery temperature in the ITMS for higher air flow rate did not alter significantly due to a little heat storage by PCM compared with pure air cooling. Fig. 13 shows the heat dissipation ratios of the PCM and air cooling (μ) at different thermal resistance ratios (ξ). According to Eq. (15), μ>1 indicated that the explicit heat storage of PCM prevailed. For the air flow rate of 18 m^3/h, the heat dissipation ratio was just equal to 0.46, which means that the battery cooling was primarily dependent on air convection and the influence of PCM was not significant. However, considering the energy saving, it was desirable that the PCM exerted major influence in the ITMS. Many methods can be taken to enhance the heat exchange between the cell and the PCM, such as increasing the thermal conductivity of the PCM by infiltrating the paraffin into the foam metal or mixing the powder material with high thermal conductivity, reducing the contact resistance. During the discharge process, the PCM absorbed most of the generation heat of the battery to increase the energy utilization rate of the battery pack as much as possible. Compared with the charging process, it is a good option to increase the air velocity to reduce the convective thermal resistance due to the existence of the external energy. The working time of the PCM could be greatly improved and the initial temperature of the battery could be decreased rapidly in the discharge process.

4.3.4. Effect of excess melting temperature of PCM

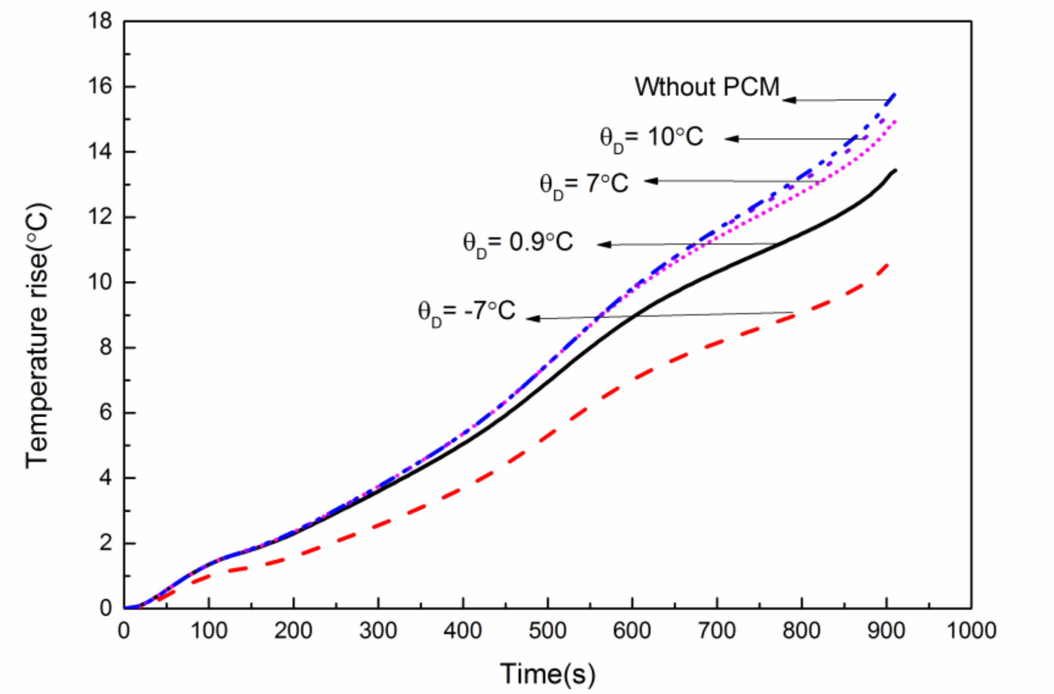

Fig. 14. The effect of the excess melting temperature of the PCM on the battery temperature rise.

The effect of the excess melting temperature of PCM on the battery temperature rise under natural convection is shown in Fig. 14. Excess melting temperature (θ_D) is equal to the melting temperature above the ambient temperature. As the excess melting temperature increased from

-7 °C to 10 °C, the maximum temperature rise went up from 11 to 15.6 °C. This indicates that the lower θ_D has a positive effect on reducing the battery temperature rise. According to Eq. (15), the large excess melting temperature may result in less heat absorption of PCM at a fixed value of ξ. When θ_D =10 °C, the battery temperature curve was infinitely close to that of the pure air cooling due to the air cooling dominating the major heat. In order to overcome it, reducing the melting temperature and increasing the ambient temperature can be taken to enhance the heat absorption of the PCM. However, increasing the ambient temperature is easy to induce the battery overheating although the maximum temperature rise decreases. In addition, the PCMs will slowly absorb the heat from the high temperature environment, this can seriously reduce their working times. Consequently, a better approach could be that making the melting temperature of the PCM is slightly below ambient temperature, and ensures that there is no heat exchange between the PCSEU and the environment.

5. Conclusions

This paper performed a combined experimental and numerical study to investigate the ITMS with the PCM for the power battery. A mathematical model of the battery temperature for the ITMS was developed. Analyses of the experimental and theoretical results lead to the following main conclusions:

(1) Air cooling system could lead to a non-uniform temperature distribution and energy consumption. The overheating occurs in the natural convection at 42 °C. In comparison, the ITMS can effectively maintain battery temperature below 55 °C under natural convection at 35 °C and the small air flow rate at 42 °C.

(2) The temperature rise of the battery is a non-steady process for high charge/discharge

rate. The irregular variation of the heat generation power was the comprehensive influence of the battery temperature, charge/discharge current, Joule heat and reaction heat. The battery temperature rising behavior can be accurately represented by the mathematical model which can effectively make a reference to optimal design of the battery TMS.

(3) The effect of several control parameters, such as heat generation power, ambient temperature, thermal resistances, initial temperature and melting temperature on the temperature characteristic of the battery is discussed in detail. The higher initial temperature is not conducive to reduce the maximum temperature of the battery. The battery temperature can be reduced by decreasing R_h and R_p, but the latter is better for energy conservation. The lower excess melting temperature has a positive effect on reducing the battery temperature rise. In addition, the battery will not be insulated by the PCM, even if the PCM melt completely.

Acknowledgement

The authors would like to acknowledge the financial support from UoA 15 Flexible Fund from Northumbria University, United Kingdom. This work was supported by the CRRC TANGSHAN CO., LTD.

References

[1] Rao Z, Wang S, Wu M, Lin Z, Li F. Experimental investigation on thermal management of electric vehicle battery with heat pipe. Energy Conversion & Management 2013; 92-97.

[2] Putra N, Ariantara B, Pamungkas R A. Experimental investigation on performance of lithium-ion battery thermal management system using flat plate loop heat pipe for electric

vehicle application. Applied Thermal Engineering 2016; 99:784-789.

[3] Biensan P, Simon B, Pérès J. P., Guibert A, Broussely M, Bodet J. M., Perton F. On safety of lithium-ion cells. Journal of Power Sources 1999; 81-82(99):906-912.

[4] Ling Z, Chen J, Fang X, Zhang Z, Xu T, Gao X, Wang S. Experimental and numerical investigation of the application of phase change materials in a simulative power batteries thermal management system. Applied Energy 2014; 121(121):104-113.

[5] Ramadass P, Haran B, White R, Popov B. Capacity fade of Sony 18650 cells cycled at elevated temperatures: Part I. Cycling performance. Journal of Power Sources 2002; 112(2):606-613.

[6] Zolot M, Pesaran A, Mihalic M. Thermal Evaluation of Toyota Prius Battery Pack. Future Car Congress 2002.

[7] Wu M S, Liu K H, Wang Y Y, Wan C C. Heat dissipation design for lithium-ion batteries. Journal of Power Sources 2002; 109(1):160-166.

[8] Huo Y, Rao Z, Liu X, Zhao J. Investigation of power battery thermal management by using mini-channel cold plate. Energy Conversion & Management 2015; 89:387-395.

[9] Zhao J, Rao Z, Li Y. Thermal performance of mini-channel liquid cooled cylinder based battery thermal management for cylindrical lithium-ion power battery. Energy Conversion & Management 2015; 103:157-165.

[10] Khateeb S A, Farid M M, Selman J R, Al-Hallaj S. Design and simulation of a lithium-ion battery with a phase change material thermal management system for an electric scooter. Journal of Power Sources 2004; 128(2):292-307.

[11] Rao Z, Wang S, Zhang G. Simulation and experiment of thermal energy management with

phase change material for ageing $LiFePO_4$, power battery. Energy Conversion & Management 2011; 52(12):3408-3414.

[12] Yang X H, Tan S C, Liu J. Thermal management of Li-ion battery with liquid metal. Energy Conversion & Management 2016; 117:577-585.

[13] Qian Z, Li Y, Rao Z. Thermal performance of lithium-ion battery thermal management system by using mini-channel cooling. Energy Conversion & Management 2016; 126:622-631.

[14] Kelly K J, Mihalic M, Zolot M. Battery Usage and Thermal Performance of the Toyota Prius and Honda Insight during Chassis Dynamometer Testing. Battery Conference on Applications & Advances 2002; 247-252.

[15] Azizi Y, Sadrameli S M. Thermal management of a $LiFePO_4$, battery pack at high temperature environment using a composite of phase change materials and aluminum wire mesh plates. Energy Conversion & Management 2016; 128: 294-302.

[16] Khateeb S A, Amiruddin S, Farid M, Selman J R, Al-Hallaj S. Thermal management of Li-ion battery with phase change material for electric scooters: experimental validation. Journal of Power Sources 2005; 142(1):345-353.

[17] Li W, Qu Z, He Y, Tao Y. Experimental study of a passive thermal management system for high-powered lithium ion batteries using porous metal foam saturated with phase change materials. Journal of Power Sources 2014; 255(6):9-15.

[18] Somasundaram K, Birgersson E, Mujumdar A S. Thermal–electrochemical model for passive thermal management of a spiral-wound lithium-ion battery. Journal of Power Sources 2012; 203(1):84-96.

[19] Alipanah M, Li X. Numerical studies of lithium-ion battery thermal management systems using phase change materials and metal foams. International Journal of Heat & Mass Transfer 2016; 102:1159-1168.

[20] Wu W, Yang X, Zhang G, Ke X, Wang Z, Situ W, Li X, Zhang J. An experimental study of thermal management system using copper mesh-enhanced composite phase change materials for power battery pack. Energy 2016; 113:909-916.

[21] Lin C, Xu S, Chang G, Liu J. Experiment and simulation of a $LiFePO_4$, battery pack with a passive thermal management system using composite phase change material and graphite sheets. Journal of Power Sources 2015; 275:742-749.

[22] Zou H, Wang W, Zhang G, Qin F, Tian C,Yan Y. Experimental investigation on an integrated thermal management system with heat pipe heat exchanger for electric vehicle. Energy Conversion & Management 2016; 118:88-95.

[23] Tiari S, Qiu S, Mahdavi M. Discharging process of a finned heat pipe–assisted thermal energy storage system with high temperature phase change material. Energy Conversion & Management 2016; 118: 426-437.

[24] Hémery C V, Pra F, Robina J F, Marty P. Experimental performances of a battery thermal management system using a phase change material. Journal of Power Sources 2014; 270(4):349-358.

[25] Saito Y. Thermal behaviors of lithium-ion batteries during high-rate pulse cycling. Journal of Power Sources 2005; 146(1-2):770-774.

[26] Dong H J, Baek S M. Thermal modeling of cylindrical lithium ion battery during discharge cycle. Energy Conversion & Management 2011; 52(8-9):2973-2981.

[27] Bernardi D, Pawlikowski E, Newman J. A general energy balance for battery systems. Journal of the Electrochemical Society 1984; 132(1):5-12.

[28] Sato N. Thermal behavior analysis of lithium-ion batteries for electric and hybrid vehicles. Jsae Review 2000; 21(2):70-77.

[29] Duan X, Naterer G F. Heat transfer in phase change materials for thermal management of electric vehicle battery modules. International Journal of Heat & Mass Transfer 2010; 53(23-24):5176-5182.

[30] Wang CY, Srinivasan V. Computational battery dynamics (CBD)-electrochemical/thermal coupled modeling and multi-scale modeling. Journal of Power Sources 2002; 110(2):364-376.

[31] HOLMAN J P. Heat transfer. Beijing: China Machine Press; 2011, p. 119-120.